# Thermal stability of antiferroelectric-like Al:HfO<sub>2</sub> thin films with TiN or Pt electrodes

Cite as: Appl. Phys. Lett. 120, 232901 (2022); https://doi.org/10.1063/5.0083656 Submitted: 28 December 2021 • Accepted: 03 May 2022 • Published Online: 06 June 2022

🧓 Alexis Payne, 匝 H. Alex Hsain, 匝 Younghwan Lee, et al.







#### ARTICLES YOU MAY BE INTERESTED IN

Enhancement of the ferroelectricity by interface engineering observed by in situ transmission electron microscope

Applied Physics Letters 120, 232107 (2022); https://doi.org/10.1063/5.0087715

Ferroelectricity in hafnium oxide thin films

Applied Physics Letters 99, 102903 (2011); https://doi.org/10.1063/1.3634052

Sublayer thickness dependence of nanolaminated HfO2-Al2O3 films for ferroelectric phase stabilization

Applied Physics Letters 120, 222902 (2022); https://doi.org/10.1063/5.0092125

Lock-in Amplifiers up to 600 MHz



Zurich







# Thermal stability of antiferroelectric-like Al:HfO<sub>2</sub> thin films with TiN or Pt electrodes

Cite as: Appl. Phys. Lett. **120**, 232901 (2022); doi: 10.1063/5.0083656 Submitted: 28 December 2021 · Accepted: 3 May 2022 · Published Online: 6 June 2022







Alexis Payne,<sup>1,2,a)</sup> (b) H. Alex Hsain,<sup>2</sup> (b) Younghwan Lee,<sup>2</sup> (b) Nicholas A. Strnad,<sup>1</sup> Jacob L. Jones,<sup>2</sup> (b) and Brendan Hanrahan<sup>1</sup> (b)

#### **AFFILIATIONS**

- <sup>1</sup>Sensors and Electron Devices Directorate, US CCDC Army Research Laboratory, Adelphi, Maryland 20783, USA
- <sup>2</sup>Department of Materials Science and Engineering, North Carolina State University, Raleigh, North Carolina 27695, USA

#### **ABSTRACT**

HfO<sub>2</sub>-based antiferroelectric-like thin films are increasingly being considered for commercial devices. However, even with initial promise, the temperature sensitivity of electrical properties such as loss tangent and leakage current remains unreported. 50 nm thick, 4 at. % Al-doped HfO<sub>2</sub> thin films were synthesized via atomic layer deposition with both top and bottom electrodes being TiN or Pt. A study of their capacitance vs temperature showed that the Pt/Al:HfO<sub>2</sub>/Pt had a relative dielectric permittivity of 23.30  $\pm$  0.06 at room temperature with a temperature coefficient of capacitance (TCC) of  $78 \pm 86 \,\mathrm{ppm/^\circ C}$ , while the TiN/Al:HfO<sub>2</sub>/TiN had a relative dielectric permittivity of 32.28  $\pm$  0.14 at room temperature with a TCC of  $322 \pm 41 \,\mathrm{ppm/^\circ C}$ . The capacitance of both devices varied less than 6% over 1 to  $1000 \,\mathrm{kHz}$  from  $-125 \,\mathrm{to} \,125\,^\circ\mathrm{C}$ . Both capacitors maintained loss tangents under 0.03 and leakage current densities of  $10^{-9}-10^{-7} \,\mathrm{A/cm^2}$  between  $-125 \,\mathrm{mod} \,125\,^\circ\mathrm{C}$ . The TiN/Al:HfO<sub>2</sub>/TiN capacitor maintained an energy storage density (ESD) of  $18.17 \pm 0.79 \,\mathrm{J/cm^3}$  at an efficiency of  $51.79\% \pm 2.75\%$  over the  $-125 \,\mathrm{to} \,125\,^\circ\mathrm{C}$  range. The Pt/Al:HfO<sub>2</sub>/Pt capacitor also maintained a stable ESD of  $9.83 \pm 0.26 \,\mathrm{J/cm^3}$  with an efficiency of  $62.87\% \pm 3.00\%$  over the same temperature range. Such low losses in both capacitors along with their thermal stability make antiferroelectric-like, Al-doped HfO<sub>2</sub> thin films a promising material for temperature-stable microelectronics.

Published under an exclusive license by AIP Publishing. https://doi.org/10.1063/5.0083656

Antiferroelectric (AFE) materials have long been considered for energy storage applications, 1-7 but more recently, the fabrication of AFE thin films has also allowed these materials to be considered for applications such as memory,8 decoupling and filtering circuits,<sup>9</sup> and microelectromechanical systems (MEMS) actuators. 10 Although it is not the strict definition, AFEs are experimentally characterized by a double polarization electric field (PE) hysteresis loop. 11-15 The debate about the origin of this effect in the thin film HfO2 is on-going. However, as much as AFE materials have found use in certain applications, many of these materials have wide variability in their relative dielectric permittivity over relatively small temperature changes, which hinders their use in microelectronics.16 For example, the relative dielectric permittivity of thin films of PbZrO<sub>3</sub> (PZO) changes from ≈100 at 25 °C to  $\approx$ 225 at 225 °C. <sup>17</sup> AFE PbHfO<sub>3</sub> (PHO) thin films also suffer from a 300% change in the relative dielectric permittivity between 25 and 200 °C. 18 This temperature variability can be compensated for, though it requires either auxiliary components such as heat sinks or a lookup table. A lookup table is a table generated by exposing

the device to various temperatures and recording the relative permittivity, allowing for corrections to be calculated, while the device is running.  $^{16}$ 

AFE-like, doped HfO<sub>2</sub> thin films have demonstrably higher intrinsic temperature stability than their Pb-based counterparts. The term "AFE-like" as opposed to "AFE" is used because there is ongoing debate about the underlying mechanism that causes the characteristic "double PE loop" in HfO<sub>2</sub>-based films. 19-22 Several theories have been suggested such as an electric-field-driven phase transition from the non-polar tetragonal phase to the polar orthorhombic phase, <sup>19</sup> while another theory suggests a depolarization field from charged defects as the mechanism.<sup>20</sup> Some HfO<sub>2</sub>-based thin films, such as under  $\approx\!\!5$  at. % Si:HfO  $_2$  thin films and  $Hf_xZr_{1-x}O_2$  with  $x\!>\!\!0.5$  , start with an AFE-like hysteresis loop, but, as they are electrically cycled, their remanent polarization,  $P_r$ , increases. <sup>23,24</sup> This "wake-up" effect is thought to be due to the redistribution of charged defects in the thin films,<sup>21</sup> though it was also suggested that this could simply be the re-orientation of orthorhombic unit cells under applied field.<sup>22</sup> Regardless of the origin of the AFE-like response seen in these thin

a) Author to whom correspondence should be addressed: alexis.l.payne@gmail.com

films, initial work demonstrating the temperature stability of AFE-like  $HfO_2$  thin films shows a material with promising stability for temperature variable applications. 4 at. %  $Si:Hf_{0.5}Zr_{0.5}O_2$  (HZO) and 4 at. %  $Al:Hf_{0.5}Zr_{0.5}O_2$  with TiN electrodes demonstrated stable energy storage density (ESD) values of  $\approx$ 45 and  $\approx$ 25 J/cm³, respectively, from 25 to  $125\,^{\circ}$ C and up to  $10^7$  cycles. AFE-like  $Hf_{0.3}Zr_{0.7}O_2$  with TiN electrodes has also demonstrated sustained ESD values of  $\approx$ 30 J/cm³ from 25 to  $175\,^{\circ}$ C. However, other work reports some variation in  $P_r$  with temperature. For example, the  $P_r$  of 4.5 at. % Si:HfO<sub>2</sub> films increased as temperature decreased from 126 to  $-193\,^{\circ}$ C, which Park *et al.* attributed to an increase in the orthorhombic polar phase fraction of the material via grazing incidence x-ray diffraction (GIXRD). Another study reported 6 mol. % Si:HfO<sub>2</sub> thin films with TiN electrodes also experienced an increase in  $P_r$  with decreasing temperature.

To date, a robust study of the loss tangent, leakage current, and relative dielectric permittivity of these materials with temperature and frequency has yet to be reported. Prior works have also not considered the effect of electrode material on the temperature stability of HfO2 based thin films. Yet, the applicability of numerous other electrodes to HfO2 thin films has been demonstrated, a not exhaustive list of examples including HfN,<sup>27</sup> TaN,<sup>11,28</sup> RuO<sub>2</sub>,<sup>29</sup> Ni,<sup>30</sup> Pd,<sup>30</sup> W,<sup>31</sup> WN,<sup>32</sup> Ir,<sup>33</sup> and Pt,  $^{30,34}$  resulting in variations in properties such as  $P_r$  and phase composition. Newly reported results of the temperature stability of the loss tangent and leakage current using alternative electrodes, such as Pt, would further expand the design options for device architectures in which these films can be utilized. Not only such measurements would validate the ability of these materials to maintain low leakage current and loss tangent values at high temperatures, but also new investigations of the dielectric losses vs temperature could broaden the understanding of the driving mechanism for the AFE-like response that is realized in certain types of HfO2 thin films. In this study, we chose to compare 4 at. % Al:HfO2 thin films with either TiN electrodes or Pt electrodes. These electrodes were chosen as the TiN electrodes have been theorized to act as an oxygen sink for HfO2 thin films, 35 while Pt electrodes would not, enabling a comparison of HfO2 thin films with these two distinctly different types of electrodes.

The 4 at. % 50 nm Al:HfO2 thin films on Pt were prepared at the Army Research Laboratory (ARL) in Adelphi, MD, and the fabrication procedure has been described in prior work.<sup>34</sup> The substrate used was a Si substrate with a 500 nm of thermally grown SiO2. The Ti adhesion layer is sputtered and then oxidized to form a 32 nm TiO2 layer. 100 nm Pt electrodes were sputtered onto the Si/SiO<sub>2</sub>/TiO<sub>2</sub> substrate via DC magnetron sputtering. The Al:HfO2 thin films were grown using a Kurt Lesker atomic layer deposition (ALD) 150-LX system. The precursors used were tetrakis(dimethylamino)-hafnium (TDMAH) and trimethylaluminum (TMA) with H<sub>2</sub>O as the oxygen precursor. The substrate was heated at 250 °C with Ar as the inert purge gas. The ratio of the Al<sub>2</sub>O<sub>3</sub> cycles to HfO<sub>2</sub> cycles was 1:24. The first 1-2 nm of thin film was deposited, and then the sample was removed from the ALD chamber to undergo a thermal treatment in an RTA at 300 °C for 60 s in N2. This annealing step was found to improve reliability of the samples, possibly due to the removal of volatile organics at the Pt/Hf interface. The sample is then returned to the chamber to finish growth. A 100 nm Pt top electrode is sputtered onto the sample using DC magnetron sputtering, with top electrodes being defined using photolithography. The sample then underwent a rapid thermal anneal at 700 °C for 60 s in N<sub>2</sub>.

The 4 at. % 50 nm Al:HfO<sub>2</sub> thin films on TiN were prepared at the North Carolina State University Nanofabrication Facility (NNF). A 50 nm TiN bottom electrode was deposited on a Si/SiO<sub>2</sub> substrate using plasma-enhanced atomic layer deposition (PEALD). An Ultratech/Cambridge Fiji G2 system was used for the ALD growths. The precursor used was tetrakis(dimethylamido)-titanium(IV) at a pressure of ~0.1 Torr for its half-cycles and 0.01 Torr for plasma halfcycles. The Ar/N<sub>2</sub> gas was used to generate plasma, which was pulsed for 20 s at 250 W. After the TiN bottom electrode deposition, the substrate was not removed from the chamber, i.e., the samples were grown via a Sequential, No-Atmosphere Process (SNAP).35 The 50 nm Al:HfO2 was deposited using thermal ALD with TDMAH and TMA as the precursors and H<sub>2</sub>O as the oxidizer, with again a 1:24 ratio between the HfO<sub>2</sub> cycles and the Al<sub>2</sub>O<sub>3</sub> cycles. The substrate temperature was kept at 270 °C, and Ar was the inert purge gas. The TiN top electrode was then deposited onto the Al:HfO2 thin film without removing the thin film from the chamber. After deposition of the top TiN electrode, the sample then underwent a rapid thermal anneal at 700 °C for 60 s in N<sub>2</sub>. The top electrodes were defined at ARL using an ion mill (4wave 4W-PSIBE). The ion milling was conducted at a  $95^{\circ}$ etch angle with a beam voltage of 400 V, beam current of 400 mA, and an acceleration voltage of 150 V.

The polarization vs electric field (PE) loops and leakage current were measured using a Radiant Technologies Precision Premier II. The capacitor area was 0.000 492 cm<sup>2</sup>. The samples were mounted in a Lake Shore PS-100 tabletop probe station with a liquid nitrogen cooled temperature-controlled stage. The samples were mounted to the stage using thermal grease. The samples were cooled to  $-125\,^{\circ}$ C, and individual PE loop measurements, energy storage density (ESD) measurements, and leakage current measurements were made every 25 °C up to 125 °C. A 15 V bipolar PE loop was measured at 1 kHz, a monopolar hysteresis loop was measured at 1 kHz to calculate ESD and efficiency of the device at 15 V, and the current-voltage (IV) measurement was conducted using a 5 V switched linear waveform with a 1000 ms soak time. The resultant PE loops at increasing temperature for a representative single capacitor on each sample are presented in Fig. 1. The  $P_r$  and maximum polarization ( $P_{\text{max}}$ ) remain stable with increasing temperature. The  $P_{\text{max}}$  at positive voltage of the TiN/ Al:HfO<sub>2</sub>/TiN increased by 0.97  $\mu$ C/cm<sup>2</sup> from -125 to 125 °C, and  $P_r$ decreased by 0.87  $\mu$ C/cm<sup>2</sup> from -125 to 125 °C. The  $P_{\text{max}}$  of Pt/Al:HfO<sub>2</sub>/Pt increased by 0.24  $\mu$ C/cm<sup>2</sup>, and the  $P_r$  decreased by 0.27  $\mu$ C/cm<sup>2</sup> from -125 to 125 °C. The stable  $P_r$  in both capacitors suggests that the driving mechanism for the AFE-like response seen in these thin films is not affected by temperature. This result differs from prior work on Si:HfO2 thin films, which demonstrated a more significant increase in  $P_r$  with decreasing temperature. <sup>25,26</sup> The authors of those prior works attributed the increase in  $P_r$  to an increase in the orthorhombic phase. 25,26 However, in both prior works, 10 nm thick thin films were measured, and Choi et al. previously measured a decreasing orthorhombic phase fraction with increasing film thickness.<sup>36</sup> Thus, the 50 nm thin films in this work likely have lower orthorhombic phase fractions than the  $HfO_2$  thin films shown to have an increase in  $P_r$  with a decrease in temperature. The temperature stable  $P_r$  also suggests that orthorhombic phase fractions in both Pt/Al:HfO<sub>2</sub>/Pt and TiN/Al:HfO<sub>2</sub>/ TiN capacitors are stable with temperature. While both capacitors demonstrate similar temperature stability, there is a clear difference in the P<sub>max</sub> that is achieved between the Pt/Al:HfO<sub>2</sub>/Pt capacitors and the

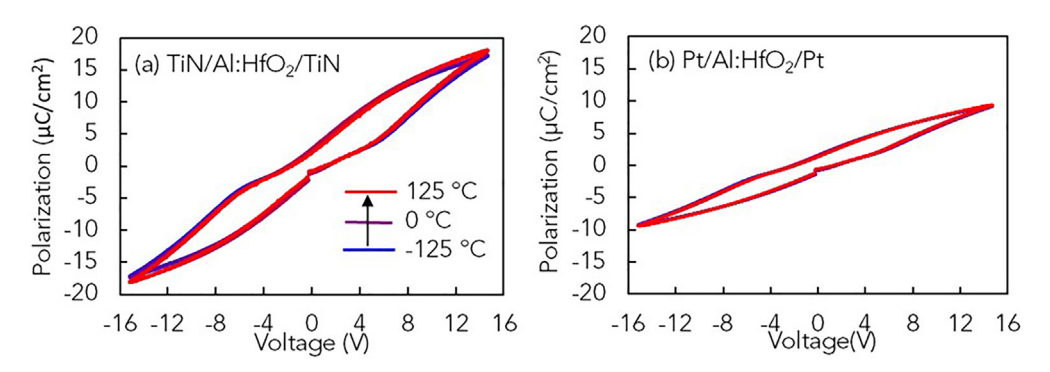


FIG. 1. PE loops of (a) TiN/50 nm 4 at. % Al:HfO<sub>2</sub>/TiN and (b) Pt/50 nm 4 at. % Al:HfO<sub>2</sub>/Pt from -125 to 125 °C at 25 °C steps.

TiN/Al:HfO<sub>2</sub>/TiN capacitors, which can be explained by considering the effect of the bottom electrode on the ferroelectric layer. Park et al. found that the use of (111)-textured Pt bottom electrodes resulted in the formation of (111)-textured  $Hf_{0.5}Zr_{0.5}O_2$  (HZO).<sup>37</sup> (111)-Textured HZO was found to suppress the phase transformation from tetragonal to orthorhombic due to unfavorable orientation of the tetragonal cell during annealing. Such an orientation caused an equivalent tensile strain state across a-, b-, and c-axes, which did not promote the formation of the orthorhombic phase. The larger o111/t011 peak intensity of the TiN/Al:HfO<sub>2</sub>/TiN capacitors relative to that of the Pt/Al:HfO<sub>2</sub>/Pt capacitors in the GIXRD patterns, Fig. S1, suggests that the TiN/ Al:HfO<sub>2</sub>/TiN capacitors have a higher orthorhombic phase fraction than the Pt/Al:HfO2/Pt capacitors. However, prior work showed the TiN/Al:HfO<sub>2</sub>/TiN capacitors fabricated via SNAP have a clean chemical interface with a diminished TiO<sub>x</sub>N<sub>v</sub> layer and carbon impurities at the electrode interfaces leading to enhanced  $P_{\rm max}$  values. <sup>35</sup> The TiO $_{\rm x}$ N $_{\rm v}$  layer typically acts as a dead layer that reduces the ferroelectric response of a material. The stability of the ESD and efficiency of the capacitors vs temperature can be seen in Fig. S2 with the TiN/Al:HfO2/TiN capacitor having a higher ESD at 18.17 ± 0.79 J/cm<sup>3</sup> than the Pt/Al:HfO<sub>2</sub>/Pt at

 $9.83\pm0.26$  J/cm³. However, due to the larger hysteresis of PE loop of TiN/Al:HfO<sub>2</sub>/TiN, it exhibits efficiency of  $51.79\%\pm2.75\%$ , which is  $\sim10\%$  lower at all temperatures relative to the Pt/Al:HfO<sub>2</sub>/Pt of  $62.87\%\pm3.00\%$ . Figure 2 shows the leakage current of both samples with increasing temperature. The leakage current measurements were conducted on capacitors with areas of  $0.001\,81\,\text{cm}^2$ . The leakage current values of  $10^{-9}-10^{-7}$  A/cm² shown in Fig. 2 are lower than values previously reported for other AFE thin films such as PZO  $(10^{-3}\text{ A/cm}^2)$ ,  $^{38}$  (Pb<sub>0.92</sub>La<sub>0.08</sub>)(Zr<sub>0.65</sub>Ti<sub>0.35</sub>)O<sub>3</sub>  $(10^{-4}\text{ A/cm}^2)$ ,  $^{39}$  and similar to our own PHO  $(10^{-8}\text{ A/cm}^2)$ . The thermal stability of the leakage current densities of the Al:HfO<sub>2</sub> capacitors also provides a significant benefit over current bulk capacitors such as tantalum capacitors and multilayer ceramic capacitors (MLCCs), which are known to have increases of two orders of magnitude or more in leakage current over the full military temperature range (-55 to  $125\,^{\circ}$ C).  $^{40}$ 

The capacitance and loss tangent values were also measured from -125 to  $125\,^{\circ}\mathrm{C}$  at  $25\,^{\circ}\mathrm{C}$  intervals using an HP4192a Impedance Analyzer with the Lakeshore probe station with temperature-controlled stage and can be seen in Fig. 3. The loss tangent is a measure of the alternating current (AC) losses in a material due to the

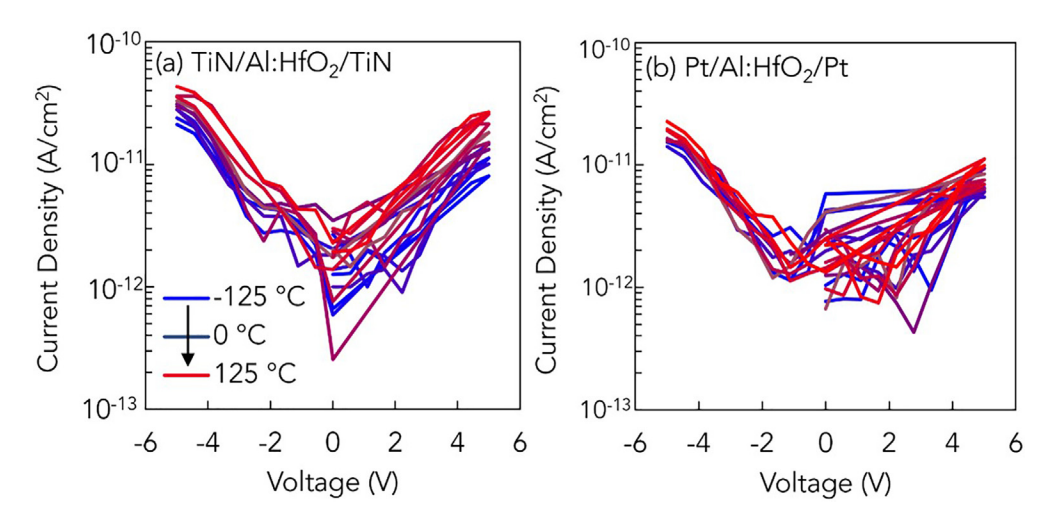


FIG. 2. Leakage current measurements of (a) TiN/50 nm 4 at. % Al:HfO<sub>2</sub>/TiN capacitor and (b) Pt/50 nm 4 at. % Al:HfO<sub>2</sub>/Pt capacitor at temperatures from -125 to 125 °C at 25 °C intervals.

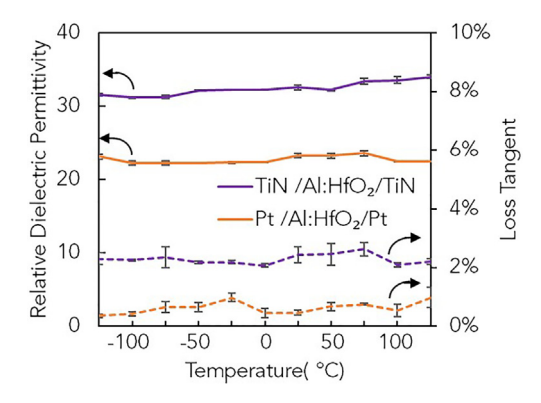


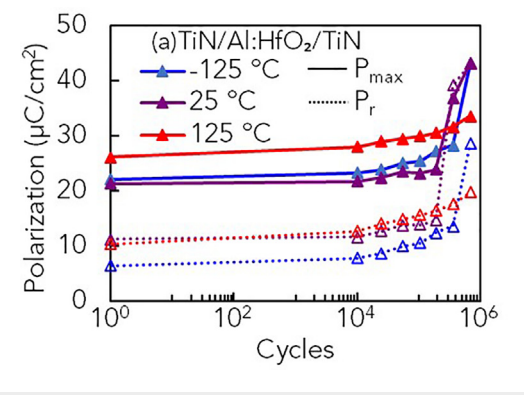
FIG. 3. Relative permittivity and loss tangent values of TiN/50 nm 4 at. % Al:HfO<sub>2</sub>/ TiN and Pt/50 nm 4 at. % Al:HfO<sub>2</sub>/Pt from -125 to  $125\,^{\circ}$ C at  $25\,^{\circ}$ C steps.

movement of atoms or molecules. The loss values remained below 0.03 for both TiN/Al:HfO2/TiN and Pt/Al:HfO2/Pt at all measured temperatures. The capacitance measurements were used to calculate the relative dielectric permittivities as well as determine the temperature coefficient of capacitance (TCC) for each of the capacitors. The TCC was calculated from the slope of the linear fit of the data. The Pt/ Al:HfO<sub>2</sub>/Pt capacitor proved to have a lower relative dielectric permittivity of 23.30 at 25 °C but also a lower TCC of  $78 \pm 86 \,\mathrm{ppm}/^{\circ}\mathrm{C}$ . The TiN/Al:HfO2/TiN capacitor had a relative dielectric permittivity of 33.70 with a larger TCC of 320 ppm/°C. These TCC values are not as high as class 1 temperature stable capacitors, which can have TCC values as low as  $0 \pm 30$  ppm, but are significantly better than class 2 dielectrics, which have TCC values in the parts per thousand per degree (ppt).<sup>42</sup> However, it should be noted that these devices would have to be packaged to be commercialized, which would affect their ultimate TCC values. Figure 3 shows an average of four measurements taken every 25 °C at 10 kHz with an AC signal of 0.1 V with 0 V bias with the standard deviation denoted with error bars. A series of capacitance vs frequency measurements were also made every 25 °C. The relative dielectric permittivity calculated from using a parallel model of a capacitor and resistor using the capacitance measurements made ranging from 1 to 1000 kHz with increasing temperature can be seen in Fig. S3. The capacitance of TiN/Al:HfO<sub>2</sub>/TiN varied less than 6% at all

frequencies and temperatures, while the capacitance of the  $Pt/Al:HfO_2/Pt$  capacitor varied less than 5% for all frequencies and temperatures measured.

Endurance cycling measurements were conducted on three separate capacitors at -125, 25, and 125 °C for each sample using a 5 V bipolar waveform. The magnitude of the waveform was selected as it mimics what could be seen as a realistic operating voltage for these materials.<sup>34</sup> However, other works have demonstrated that a larger magnitude electric field in endurance measurements can result in early breakdown and/or early onset of wake-up. 14 The variability in the starting  $P_r$  at each respective temperature is attributed to the variability from capacitor to capacitor. A PE loop and a leakage current measurement were taken before and after the endurance cycling. The change in  $P_r$  per electric field cycle,  $dP_r/dN$ , increases sharply in both capacitors after 10<sup>4</sup> cycles as shown in Fig. 4, demonstrating that each of these samples experienced wake-up whether at  $-125\,^{\circ}\text{C}$  or  $125\,^{\circ}\text{C}$ . Thus, demonstrating that both sets of samples respond in the same manner to an increase in temperature, even as the capacitors wake-up during endurance cycling. The pre- and post-endurance cycling PE loops and leakage current measurements are shown in Fig. S4, and both capacitors transitioned from AFE-like to FE response with endurance cycling. The pre- and post-wake-up leakage current did not change significantly between pre- and post-endurance cycling as is shown in Fig. S5. A measurement of the capacitance of both the Pt/ Al:HfO<sub>2</sub>/Pt and the TiN/Al:HfO<sub>2</sub>/TiN capacitors pre- and post-wakeup at room temperature also showed no change after wake-up.

As previously stated, the stability in the PE loops of these samples between -125 and  $125\,^{\circ}\mathrm{C}$  suggests that the driving mechanism for the AFE-like response in the TiN/Al:HfO2/TiN sample and the Pt/Al:HfO2/Pt sample is fairly temperature insensitive. The temperature stability of the polarization suggests that the driving mechanism for the AFE-like response in this material is unlikely to be caused by an electrically induced phase transition from tetragonal phase to orthorhombic phase since the tetragonal phase is the high temperature phase. The lack of a change in the permittivity of the material pre- and post-endurance cycling further suggests that the driving mechanism for wake-up in these samples is likely not a change in phase composition. The permittivity of the orthorhombic phase for HfO2 has been previously reported as  $30,^{43}$  while the tetragonal phase has been reported as  $35-40.^{44}$  The lack of a shift in the permittivity suggests



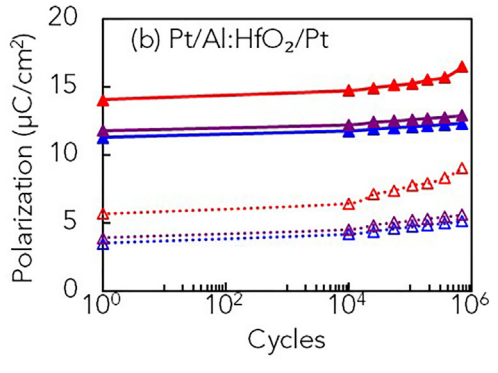


FIG. 4. Remanent polarization (P<sub>r</sub>) and maximum polarization (P<sub>max</sub>) vs number of cycles for (a) TiN/50 nm 4 at. % Al:HfO<sub>2</sub>/TiN and (b) Pt/50 nm 4 at. % Al:HfO<sub>2</sub>/Pt at -125, and 125 °C.

that an electric-field induced phase transition is likely not the main driving mechanism for the AFE-like response. Instead, the driving mechanism could be due to the ferroelectric/ferroelastic reorientation of orthorhombic domains' polar axis with endurance cycling.<sup>22</sup> The Pt/Al:HfO2/Pt capacitor and the TiN/Al:HfO2/TiN capacitor both experience different amplitudes of  $dP_r/dN$ . However, larger values of  $dP_r/dN$  can be seen after  $10^4$  cycles for both capacitors. Though the TiN/Al:HfO<sub>2</sub>/TiN capacitor experienced a larger  $dP_r/dN$  than that of the Pt/Al:HfO<sub>2</sub>/Pt capacitor after  $10^4$  cycles. The  $dP_r/dN$  of Pt/ Al:HfO<sub>2</sub>/Pt is affected by temperature, with the quickest  $dP_r/dN$ occurring at 125 °C. Temperature dependent wake-up has also been previously noted in Y:HfO<sub>2</sub>, with both  $P_r$  prior to electric field cycling and  $P_r$  post-electric field cycling increasing with temperature.<sup>21</sup> The increase in  $dP_r/dN$  was attributed to mobile charge defects, specifically oxygen vacancies.<sup>21</sup> The larger  $dP_r/dN$  after  $10^4$  cycles in the TiN/Al:HfO<sub>2</sub>/TiN capacitor as compared to the Pt/Al:HfO<sub>2</sub>/Pt capacitor is likely due to an increased number of oxygen vacancies due to the TiN acting as an oxygen sink unlike the Pt. Thus, the higher  $dP_r/dN$ in the TiN/Al:HfO2/TiN and Pt/Al:HfO2/Pt capacitors could be understood by increased movement of charged defects at higher temperatures. The hypothesis of increased defects at higher temperatures is also supported by a small but distinctive increase in the leakage current from pre- to post-wake-up. Even though the leakage current density values of both capacitors demonstrate strong stability as compared to MLCCs from -125 to 125 °C, the TiN/Al:HfO<sub>2</sub>/TiN capacitor has a slightly larger temperature dependence than the Pt/Al:HfO2/Pt capacitors, which could indicate more mobile charge defects present in the sample. This increase in mobile charge defects in the TiN/ Al:HfO<sub>2</sub>/TiN capacitors could be due to the oxygen sink nature of the electrodes. Differences in the work functions of electrodes could also be the source of the observed differences in the leakage current. The current density asymmetry with bias for both samples (Fig. 2) suggests that there are some influences from the electrodes. Prior work by Park et al. with Hf<sub>0.5</sub>Zr<sub>0.5</sub>O<sub>2</sub> thin films determined that the dominant current conduction mechanism was Poole-Frenkel emission, which is related to volumetric defects. 45 Again, suggesting that the larger spread in TiN/Al:HfO2/TiN leakage current with increasing temperature could be equated with larger concentrations of defects.

Thin films of Al:HfO2 with either TiN electrodes or Pt electrodes are promising AFE-like architectures that exhibit enhanced temperature stability relative to other AFE materials. Their leakage current remains between  $10^{-9}$  and  $10^{-7}$  A/cm<sup>2</sup> from -125 to 125 °C. The ESD and efficiencies are also temperature-stable between -125 and 125 °C. The TiN/Al:HfO<sub>2</sub>/TiN had the highest relative dielectric permittivity, ranging from 31.56 at -125 °C to  $34.00 \pm 0.48$  at 125 °C and a TCC of 322 ± 41 ppm/°C as well as the highest ESD value of  $18.17 \pm 0.79$  J/cm<sup>3</sup>. The Pt/Al:HfO<sub>2</sub>/Pt had a more stable capacitance versus temperature with a TCC of only 78 ± 86 ppm/°C and a lower relative dielectric permittivity of 23.30  $\pm$  0.25 at 25 °C. The endurance cycling of these capacitors at various temperatures revealed a wake-up effect in the  $P_r$ . The changes in leakage current and the increased rate of wake-up with cycle number  $(dP_r/dN)$  for the TiN/Al:HfO<sub>2</sub>/TiN capacitors indicate that the movement of charged defects was the mechanism driving the wake-up phenomenon. The TiN/Al:HfO2/TiN capacitors also had larger  $dP_r/dN$  value after  $10^4$  cycles than that of the Pt/Al:HfO<sub>2</sub>/Pt capacitors, indicative of more mobile charge defects. The low leakage current values and loss tangent values along with the

low TCC values of the TiN/Al:HfO<sub>2</sub>/TiN and Pt/Al:HfO<sub>2</sub>/TiN devices highlight the potential of these thin films for commercial devices, which require superior temperature stability.

See the supplementary material for XRD data, energy storage density data, dielectric constant data as well as data on the leakage current density and hysteresis pre- and post-endurance cycling of the studied Al-doped HfO<sub>2</sub> thin films.

This project was supported in part by a fellowship at the U.S. CCDC Army Research Laboratory, administered by Oak Ridge Associated Universities (ORAU) through the U.S. Department of Energy Oak Ridge Institute for Science and Education. A.P. and J.J. acknowledge partial support from the National Science Foundation under Award No. CMMI-1634955. This work benefited from collaboration with the National Science Foundation, as part of the Center for Dielectrics and Piezoelectrics under Grant Nos. IIP-1841453 and IIP-1841466. H.A.H. was supported by the National Science Foundation Graduate Research Fellowship Program (No. DGE-1746939). This work was also partially performed at the Analytical Instrumentation Facility (AIF) at the North Carolina State University and NC State Nanofabrication Facility (NNF), which are supported by the State of North Carolina and the National Science Foundation (Award No. ECCS-2025064).

## AUTHOR DECLARATIONS Conflict of Interest

The authors have no conflicts to disclose.

## **DATA AVAILABILITY**

The data that support the findings of this study are available within the article and its supplementary material.

### **REFERENCES**

- <sup>1</sup>E. Sawaguchi, H. Maniwa, and S. Hoshino, Phys. Rev. **83**(5), 1078 (1951).
- <sup>2</sup>B. Jaffe, Proc. IRE **49**(8), 1264 (1961).
- <sup>3</sup>I. Burn and D. M. Smyth, J. Mater. Sci. 7, 339 (1972).
- <sup>4</sup>X. Hao, J. Zhai, and X. Yao, J. Am. Ceram. Soc. **92**(5), 1133 (2009).
- <sup>5</sup>M. H. Park, H. J. Kim, Y. J. Kim, T. Moon, K. D. Kim, and C. S. Hwang, Adv. Energy Mater. 4(16), 1400610 (2014).
- <sup>6</sup>J. Wei, T. Yang, and H. Wang, J. Eur. Ceram. Soc. **39**(2), 624 (2019).
- <sup>7</sup>K. Huang, G. Ge, F. Yan, B. Shen, and J. Zhai, Adv. Electron. Mater. **6**(4), 1901366 (2020).
- <sup>8</sup>M. Pešić and U. Schroeder, in *Ferroelectricity in Doped Hafnium Oxide: Materials, Properties and Devices*, edited by U. Schroeder, C. S. Hwang, and H. Funakubo (Woodhead Publishing, 2019), p. 425.
- <sup>9</sup>B. Xu, N. G. Pai, P. Moses, and L. Eric Cross, MRS Proc. **493**, 403 (1997).
- 10 M. D. Nguyen and G. Rijnders, Thin Solid Films 697, 137843 (2020).
- <sup>11</sup>P. D. Lomenzo, Q. Takmeel, C. Zhou, C. M. Fancher, E. Lambers, N. G. Rudawski, J. L. Jones, S. Moghaddam, and T. Nishida, J. Appl. Phys. 117(13), 134105 (2015)
- <sup>12</sup>R. Materlik, C. Künneth, and A. Kersch, J. Appl. Phys. 117(13), 134109 (2015).
- <sup>13</sup>X. Sang, E. D. Grimley, T. Schenk, U. Schroeder, and J. M. LeBeau, Appl. Phys. Lett. **106**(16), 162905 (2015).
- <sup>14</sup>F. Huang, X. Chen, X. Liang, J. Qin, Y. Zhang, T. Huang, Z. Wang, B. Peng, P. Zhou, H. Lu, L. Zhang, L. Deng, M. Liu, Q. Liu, H. Tian, and L. Bi, Phys. Chem. Phys. 19(5), 3486 (2017).
- <sup>15</sup>D. Zhou, J. Xu, Q. Li, Y. Guan, F. Cao, X. Dong, J. Müller, T. Schenk, and U. Schröder, Appl. Phys. Lett. **103**(19), 192904 (2013).

- <sup>16</sup>J. M. Puder, I. Kierzewski, V. F. Tseng, R. R. Knight, J. S. Pulskamp, and J. L. Martin, paper presented at the 2019 IEEE International Symposium on Inertial Sensors and Systems (INERTIAL), 2019.
- <sup>17</sup>J. Zhai and H. Chen, Appl. Phys. Lett. **82**(16), 2673 (2003).
- <sup>18</sup>B. Hanrahan, C. Milesi-Brault, A. Leff, A. Payne, S. Liu, M. Guennou, and N. Strnad, APL Mater. 9(2), 021108 (2021).
- <sup>19</sup>P. D. Lomenzo, C.-C. Chung, C. Zhou, J. L. Jones, and T. Nishida, Appl. Phys. Lett. 110(23), 232904 (2017).
- <sup>20</sup>P. D. Lomenzo, C. Richter, T. Mikolajick, and U. Schroeder, ACS Appl. Electron. Mater. 2(6), 1583 (2020).
- <sup>21</sup>S. Starschich, S. Menzel, and U. Böttger, Appl. Phys. Lett. 108(3), 032903 (2016).
- <sup>22</sup>C. Mart, T. Kämpfe, R. Hoffmann, S. Eßlinger, S. Kirbach, K. Kühnel, M. Czernohorsky, L. M. Eng, and W. Weinreich, Adv. Electron. Mater. 6(3), 1901015 (2020).
- 23T. S. Böscke, J. Müller, D. Bräuhaus, U. Schröder, and U. Böttger, Appl. Phys. Lett. 99(10), 102903 (2011).
- <sup>24</sup>M. H. Park, Y. H. Lee, H. J. Kim, T. Schenk, W. Lee, K. D. Kim, F. P. G. Fengler, T. Mikolajick, U. Schroeder, and C. S. Hwang, Nanoscale 9(28), 9973 (2017).
- <sup>25</sup>M. H. Park, C.-C. Chung, T. Schenk, C. Richter, M. Hoffmann, S. Wirth, J. L. Jones, T. Mikolajick, and U. Schroeder, Adv. Electron. Mater. 4(4), 1700489 (2018).
- <sup>26</sup>F. Ali, X. Liu, D. Zhou, X. Yang, J. Xu, T. Schenk, J. Müller, U. Schroeder, F. Cao, and X. Dong, J. Appl. Phys. **122**(14), 144105 (2017).
- <sup>27</sup>B. Zeng, W. Xiao, J. Liao, H. Liu, M. Liao, Q. Peng, S. Zheng, and Y. Zhou, IEEE Electron Device Lett. 39(10), 1508 (2018).
- <sup>28</sup>M. Hoffmann, U. Schroeder, T. Schenk, T. Shimizu, H. Funakubo, O. Sakata, D. Pohl, M. Drescher, C. Adelmann, R. Materlik, A. Kersch, and T. Mikolajick, J. Appl. Phys. 118(7), 072006 (2015).
- <sup>29</sup>S. S. Fields, S. W. Smith, S. T. Jaszewski, T. Mimura, D. A. Dickie, G. Esteves, M. David Henry, S. L. Wolfley, P. S. Davids, and J. F. Ihlefeld, J. Appl. Phys. 130(13), 134101 (2021).

- 30Y.-C. Lin, F. Mcguire, and A. D. Franklina, J. Vac. Sci. Technol. B 36(1), 011204 (2018).
- <sup>31</sup>A. Kashir, S. Oh, and H. Hwang, Adv. Eng. Mater. **23**(1), 2000791 (2021).
- <sup>32</sup>M. Si, X. Lyu, P. R. Shrestha, X. Sun, H. Wang, K. P. Cheung, and P. D. Ye, Appl. Phys. Lett. **115**(7), 072107 (2019).
- <sup>33</sup>T. Shimizu, T. Yokouchi, T. Shiraishi, T. Oikawa, P. S. Sankara Rama Krishnan, and H. Funakubo, Jpn. J. Appl. Phys., Part 1 53(9S), 09PA04 (2014).
- 34A. Payne, O. Brewer, A. Leff, N. A. Strnad, J. L. Jones, and B. Hanrahan, Appl. Phys. Lett. 117(22), 221104 (2020).
- <sup>35</sup>Y. Lee, H. Alex Hsain, S. S. Fields, S. T. Jaszewski, M. D. Horgan, P. G. Edgington, J. F. Ihlefeld, G. N. Parsons, and J. L. Jones, Appl. Phys. Lett. 118(1), 012903 (2021).
- <sup>36</sup>S.-N. Choi, S.-E. Moon, and S.-M. Yoon, Ceram. Int. 45(17), 22642 (2019).
- <sup>37</sup>M. H. Park, H. J. Kim, Y. J. Kim, T. Moon, and C. S. Hwang, Appl. Phys. Lett. 104(7), 072901 (2014).
- <sup>38</sup>M. J. Chen, X. K. Ning, S. F. Wang, and G. S. Fu, Nanoscale 11(4), 1914 (2019).
- <sup>39</sup>B. Sun, M. Guo, M. Wu, Z. Ma, W. Gao, H. Sun, and X. Lou, Ceram. Int. 45(16), 20046 (2019).
- AVX Corporation, Low Leakage Current Aspect of Designing with Tantalum and Niobium Oxide Capacitors, edited by R. Faltus (AVX Corporation, 2021).
   AVX Corporation, "COG general specifications datasheet."
- <sup>42</sup>AVX Corporation, "X7R dielectric general specifications."
- <sup>43</sup>J. Müller, T. S. Böscke, U. Schröder, S. Mueller, D. Bräuhaus, U. Böttger, L. Frey, and T. Mikolajick, Nano Lett. 12(8), 4318 (2012).
- <sup>44</sup>M. H. Park, H. J. Kim, Y. J. Kim, W. Lee, T. Moon, and C. S. Hwang, Appl. Phys. Lett. **102**(24), 242905 (2013).
- <sup>45</sup>M. H. Park, H. J. Kim, Y. J. Kim, T. Moon, K. D. Kim, Y. H. Lee, S. D. Hyun, and C. S. Hwang, J. Mater. Chem. C 3(24), 6291 (2015).